Scientia Iranica A (2014) 21(1), 19–29

SCIENTIA IRANICA

Sharif University of Technology
Scientia Iranica
Transactions A: Civil Engineering
www.scientiairanica.com

Numerical modeling of fault rupture propagation through two-layered sands

M. Mortazavi Zanjani and A. Soroush*

Department of Civil and Environmental Engineering, Amirkabir University of Technology, Tehran, P.O. Box 15875-4413, Iran.

Received 15 August 2012; received in revised form 19 May 2013; accepted 22 July 2013

KEYWORDS
Fault rupture propagation;
Numerical modeling;
Two-layered sand;
Rupture refraction.

Abstract. The fault rupture propagation phenomenon, spreading from the base rock through different layers of soil, is a matter of concern in many natural and man-made soil structures. The focus of this paper is to investigate reverse fault rupture propagation through two layers of sand deposit by means of numerical modeling. For this purpose, analyses are carried out for different permutations of three typical materials: dense sand, medium dense sand and loose sand, considering five fault dip angles: 30, 45, 60, 75 and 90 degrees, respectively. The validity of the numerical model was verified by simulating an experimental model of a homogeneous soil layer subjected to reverse faulting. Further to the general trends found in fault rupture propagation in a single layer of soil, special attention is devoted to the refraction of the fault path in the interface of two materials, as well as its concavity in the continuation. Moreover, four patterns of fault rapture propagation in two-layered sands, depending on their arrangements and fault dip angles, were concluded from the results.

1. Introduction

Fault rupture propagation through soil has been studied by researchers in sequential steps. First and foremost, fault rupture propagation through a uniform horizontal soil layer received plenty of attention in previous research. Pertinent field investigations have focused mainly on the evidence from surface and trench observations [1-2], whereas physical models [1,3-6] and numerical studies [4,6-12] have attempted to examine the direction and pattern of fault propagation in the top soil layer. Table 1 summarizes the numerical studies carried out on this subject [13-16]. Thereafter, investigations on fault rupture-soil-foundation interaction provided profound insight into the rupture mechanism [10,11,17-19].

A step forward may be the study of fault rupture in layered soils, as many natural and man-made soil structures are comprised of layers with dissimilar materials, such as distinguishable layers of sediment laid through ages in natural deposits and intentionally zoned areas in embankments and earth dams. Hence, probable changes in the rupture path due to the variations of material may be elucidated.

Until now, little information has been available on the response of layered soils to fault rupture. Considering the differences of materials, Bray et al. [20] highlighted the refraction of fault planes to steeper orientations while entering from bedrock to the overlying colluvium in normal faults. Moreover, Anastasopoulos et al. [9] reported refraction of dip-slip faults at the soil-rock interface to a steeper orientation. In a geological cross section of the Chelungpu fault [21], the fault rupture did not follow a single curvature, as previously seen in uniform layers, but experienced orientation and concavity variations while traversing different layers. Figure 1 depicts an example of rupture propagation in naturally colored soil layers exposed by a roadside

*. *Corresponding author. Tel.: 02164543009;*
E-mail addresses: mortazavim@aut.ac.ir (M. Mortazavi Zanjani) and soroush@aut.ac.ir (A. Soroush)

Table 1. Summary of numerical studies of fault rupture propagation through soils.

Reference	Constitutive law	Overlying stratum	Fault type*
Scott, Schoustra [13]	Linear elastic perfect plastic with Mohr-Coulomb failure criteria	Alluvium	N-R
Roth et al. [14]	Modified Drucker Prager, no-tension material	Alluvium	R
Walters, Thomas [15]	Drucker Prager, variable non-assoc. law, softening	Sand	DBD
Bray et al. [7]	Hyperbolic pressure dependent model for total stress analysis	Clay	N-R
Nakai et al. [16]	Elasto-plastic with volumetric response, variable dilation	Clay, Sand	DBD
Lazarte [4]	Elastic, hyperbolic, Modified Cam-Clay, elasto-plastic with modified Von Mises, assoc. flow rule and nonlinear isotropic softening	Clay	SS
Lin et al. [6]	Linear elastic perfect plastic with Mohr-coulomb failure criteria	Sand	R
Anastasopoulos et al. [9]	Elastoplastic Mohr-Coulomb constitutive model with isotropic strain softening	Sand	N-R
Johansson, Konagai [8]	Hypoplastic constitutive law	Sand	DBD
Loukidis et al. [12]	Elastoplastic Mohr-Coulomb constitutive model with strain softening for dense sand	Clay, Sand	N-R

*Key: SS= Strike Slip, N=Normal fault, R=Reverse fault, DBD=Differential Base Displacement.

Figure 1. Fault rupture in a layered ground; side trench in the Zanjan-Tabriz road, Iran (courtesy of Dr. A. Ghalandarzadeh).

trench on the Zanjan-Tabriz road, North West of Iran. The soil type is alternating depositional layers of claystone (or mudstone) and conglomerate, and the fault mechanism seems to be predominantly normal. The figure shows that the rupture path is subjected to changes as it passes through different layers of soils.

The present study tackles the key issue of finding out the fault rupture pattern in two-layered sand deposits by means of numerical modeling. In the first place, the general trends of reverse fault rupture propagation in uniform sandy soils are pursued in two-layered sands. Then, the effect of the interface between the two layers, which is deemed as a limiting boundary, on the curvature and concavity of the rupture path is studied. The capability of the numerical method is verified through simulating a series of physical modeling of uniform soils with a 100 g centrifuge apparatus. The analyses results are presented in the forms of contours of maximum shear strain rate and their core lines, as representatives of rupture paths. It is shown that soil characteristics play a major role in the refraction of rupture in the interface of two materials. Finally, the combined effects of soil type and fault dip angle on the pattern of rupture are explored and discussed.

2. Problem description and modeling

For the simulation of reverse fault rupture propagation through a two-layered sandy deposit, a 10 m high representative two dimensional cross section perpendicular to the fault plane is considered, as shown in Figure 2(a). An ample width to height ratio of five is considered for the model to exclude boundary condition effects for a wide range of fault dip angles. Considering a similar geometry in the third dimension, plane strain conditions govern. The fault movement, developed in the rigid bedrock, reaches the bedrock-soil interface at the base of the model. In order to simulate the fault movement, the right part of the model (footwall) is

Table 2. Soil parameters used in numerical simulation.

Material	Abbreviation	γ (kN/m^3)	c (kPa)	φ_p (°)	φ_{res} (°)	ψ_p (°)	ψ_{res} (°)	E (MPa)	ν
Loose sand	LS	18	5	30	30	0	0	10	0.3
Medium dense sand	MS	19	5	38	33	8	3	20	0.3
Dense sand	DS	20	5	46	36	16	6	40	0.3

Key: γ=Unit weight, c=Cohesion, φ_p, ψ_p=Ultimate mobilized friction and dilation angles, $\varphi_{\text{res}}, \psi_{\text{res}}$=Residual friction and dilation angles, E=Elastic modulus and ν=Poisson's ratio.

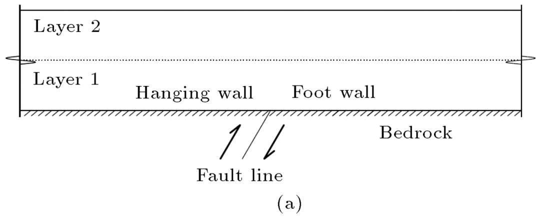

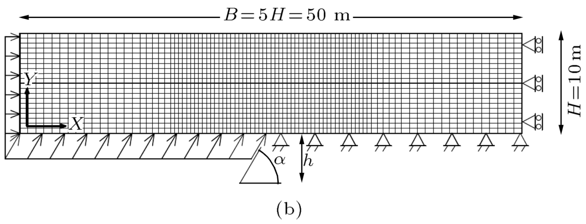

Figure 2. (a) A two-layered soil model. (b) Boundary conditions and typical meshing of the model.

fixed and movement is applied to the left bottom and left vertical side (hanging wall) of the model.

For the soil layers, three typical sands are introduced: Loose Sand (LS), Medium dense Sand (MS) and Dense Sand (DS). The input values for the physical and mechanical properties of the materials are presented in Table 2. Six different arrangements of three materials are plausible for a two-layered deposit. To name these cases, the name of the lower layer comes first; for instance, LS-DS means that the layer of loose sand is overlaid by the layer of dense sand.

Figure 2(b) shows finite element idealization of the model. The domain is discretized with quadrilateral elements similar to the previous numerical simulations [7,9,12], with a linear geometric order, which results in better numerical convergences. Based on the sensitivity analyses, whose results will be presented in the coming section, finer elements are generated for the central part (2H wide) of the model [7,9]. The model comprises 121×40 elements for fault dip angles of $\alpha = 30°, 45°, 60°$, and 152×40 elements for $\alpha = 75°, 90°$, as, for the latter, the rupture path is very steep and requires more elements in the central part for a better prediction of deformation fields.

Before imposing the fault displacement, the initial state of stress was set up in the soil. The present study is limited to dry sand and monotonic loading induced by faulting; in other words, the potential effects of strong ground motion and hydraulic effects are not in the scope of this paper. Thereafter, the base displacement was applied incrementally. In this regard, various studies have been carried out to determine the required base displacement for completion of rupture propagation. According to Cole and Lade [3], a vertical displacement of approximately 4% of the total height of the soil mass is required to complete the development of the failure surface in sands. The suggestion of Bray et al. [1] in their experiments was the vertical displacement of 2% to 6% of depth of the overlying sand layer. Loukidis et al. [12] found a displacement of 2.75% of the model height necessary for rupture to reach the surface. Our preliminary analyses suggested a vertical displacement of 4% of the soil height.

3. Constitutive model

Several constitutive models have been proposed to simulate the evolution of shear deformations induced by faults. A hyperbolic nonlinear elastic constitutive law was utilized for modeling saturated clay by Bray et al. [7]. For numerical simulation of sandy deposits, Lin et al. [6] adopted the trishear model with the elastic-perfect plastic Mohr-Coulomb constitutive behavior, and others [9,12] utilized the elastoplastic Mohr–Coulomb constitutive model with isotropic strain softening. A hypoplastic constitutive law was used by Johansson and Konagai [8].

The previous studies show that considering the post-peak soil behavior plays a determining role in describing fault rupture propagation [9,12]. In the present research, the elastoplastic Mohr-Coulomb constitutive model with isotropic strain softening and a non-associated flow rule has been incorporated [22,23]. The strain softening behavior is modeled in the finite element code Abaqus [23] through a user defined subroutine by a gradual reduction of friction and dilation angles, φ, ψ, with the increase of the plastic shear strain γ^p (Figure 3), as follows:

$$\varphi = \left\{ \begin{array}{ll} \varphi_p - \frac{\varphi_p - \varphi_{\text{res}}}{\gamma_f^p}\gamma^p & \text{for} \quad 0 \le \gamma^p < \gamma_f^p \\ \varphi_{\text{res}} & \text{for} \quad \gamma^p \ge \gamma_f^p \end{array} \right\}, \tag{1}$$

$$\psi = \left\{ \begin{array}{ll} \psi_p \left(1 - \frac{\gamma^p}{\gamma_f^p}\right) & \text{for} \quad 0 \le \gamma^p < \gamma_f^p \\ \psi_{\text{res}} & \text{for} \quad \gamma^p \ge \gamma_f^p \end{array} \right\}, \tag{2}$$

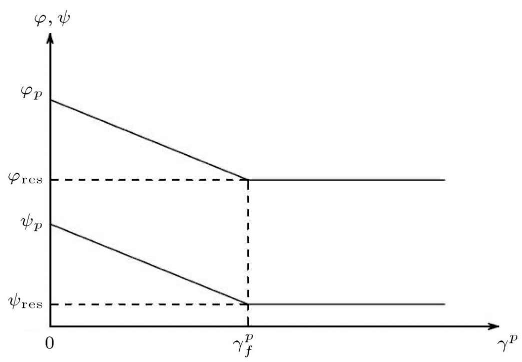

Figure 3. Variation of friction and dilation angles with plastic shear strain.

where φ_p and ψ_p are ultimate mobilized friction and dilation angles and φ_{res} and ψ_{res} are residual friction and dilation angles; γ_f^p is the plastic shear strain at which the softening is completed.

3.1. Mesh dependency

To assure a realistic description of rupture, mesh dependency is investigated from two different viewpoints of mesh density and mesh structure. The results are compared in the form of maximum shear strain rate contours for four different mesh sizes: 0.20, 0.25, 0.50 and 0.75 m. Typical results for $\alpha = 60°$ reverse fault in the dense sand are shown in Figure 4(a), while Figure 4(b) depicts the cores of these contours as the loci of the maximum shear strain rate. The results suggest that the shear zone of 0.75 m mesh size is diffused, while 0.50 and 0.25 m meshes give comparatively concentrated shear bands. The shear band of 0.20 m mesh is slightly narrower than that of 0.25 m, but at the expense of higher computational effort. Thus, the mesh size of 0.25 m was deemed optimal.

Also, the effect of mesh structure on the rupture path was studied by considering structured and unstructured meshes with 0.25 m elements. The acceptably similar rupture paths showed the independency of the path to the mesh arrangements.

3.2. Verification

To verify the capability of the numerical method and FE code to capture realistic soil behavior, the centrifuge experiments by Anastasopoulos et al. [9] have been numerically modeled.

In these tests, the length, height and width of soil specimens are 0.68, 0.25 and 0.20 m, respectively, representing a $68 \times 25 \times 20$ m specimen considering the 100 g centrifuge acceleration. The input values for the sandy soil were suggested as $\varphi = 39°$, $\psi = 11°$ and E varying in depths from 1 to 50 MPa [9]. Reverse faulting with four values of vertical displacement, h, was applied to the right side of the soil box.

Figure 5 compares the numerical and experimental results in terms of the vertical displacements of the soil surface after faulting. It is evident from this figure

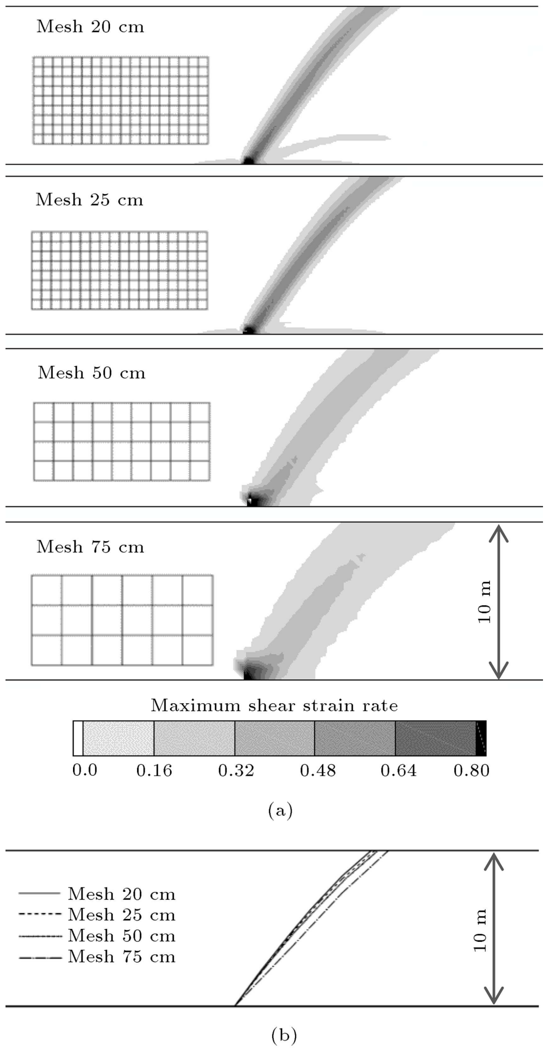

Figure 4. Effect of mesh size on fault rupture propagation and rupture path for 60° reverse fault in dense sand: (a) Contours of maximum shear strain rate; and (b) rupture path.

that the error increases with an increase in the value of h. This can be explained on the basis of experimental observations [5]. In the early stages of rupture development, a single rupture path forms inside the soil body. This results in a smooth curvature on the soil surface, being easily predictable by numerical modeling. As the base displacement increases, multiple rupture paths develop within the soil profile, resulting in small local irregularities on the main curvature of the soil surface. The experimental results for $h = 1.13$ m in Figure 5 shows such irregularities. However, as this figure indicates, the overall prediction of the surface displacement profile remains satisfactory.

4. Results

4.1. Immediate results

The outcome of numerical modeling, including stresses

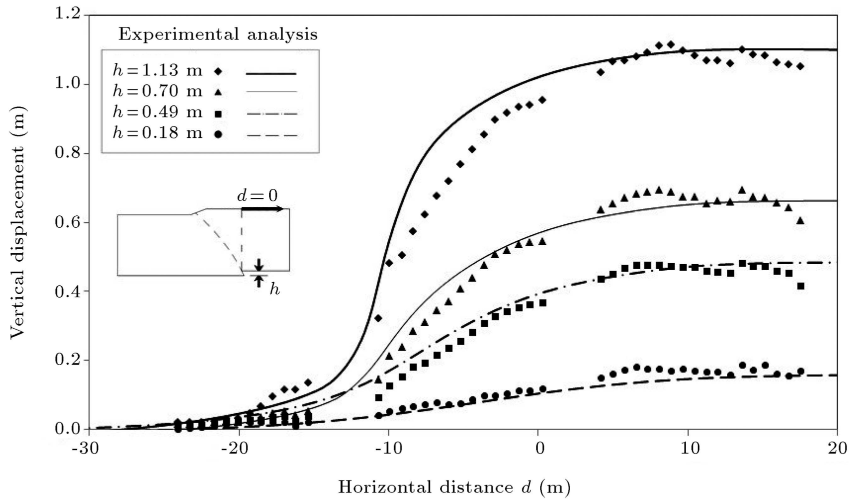

Figure 5. Reverse faulting at 60° with imposed bedrock dislocation, h, from 0.18 to 1.13 m: Comparison of vertical displacement of surface in this numerical simulation with experimental results of Anastasopoulos et al. [13].

and strains, may be related to the physical concept of fault rupture. Different researchers have used different results to pursue fault rupture paths. Bray et al. [1] used contours of shear stress and maximum shear strain, while Lazarte [4] offered maximum shear stress contours. In [6,12], plastic strains and rates of maximum shear strain contours were preferred, respectively.

Generally speaking, the stress interpretations of rupture are diffused and, therefore, cannot locate a localized zone, whereas the strain interpretations depict localized paths. Areas with high shear stress include points with relatively negligible strain rates, which make the definition of the rupture surface, in terms of stress yield factors, obscure [12]. Results of our preliminary analyses confirmed this issue. Among the strain descriptions of fault rupture, maximum shear strain and maximum shear strain rate are considered as better representatives of the fault rupture path [12].

However, special attention should be paid to the notion of maximum shear strain and maximum shear strain rate. In a static nonlinear analysis, simulation takes place over a finite period of time, t, although this time has no physical meaning. The ratio of time increment to analysis time specifies the proportion of load being applied in each increment.

$$\text{load increment} = \frac{\Delta t}{t} \times \text{load magnitude}. \tag{3}$$

The total step time is usually set to 1.0 for convenience. Base displacement is applied in small increments and maximum shear strain at each point in the increment, i, is defined as:

$$\gamma_{\max}{}^{i} = \varepsilon_{\max}{}^{i} - \varepsilon_{\min}{}^{i}, \tag{4}$$

where $\varepsilon_{\max}{}^{i}$ and $\varepsilon_{\min}{}^{i}$ are maximum and minimum strains.

Maximum shear strain rate demonstrates the instantaneous maximum shear strain at the desired increment:

$$\dot{\gamma}^{i}_{\max} = \frac{\gamma_{\max}{}^{i} - \gamma_{\max}{}^{i-1}}{\Delta t} = \frac{(\varepsilon_{\max}{}^{i} - \varepsilon_{\min}{}^{i}) - (\varepsilon_{\max}{}^{i-1} - \varepsilon_{\min}{}^{i-1})}{\Delta t}. \tag{5}$$

As reported by Loukidis et al. [12], comparing various failure indices in the numerical simulation of the Nikomidino fault in Greece showed that contours of maximum shear strain rate ($\dot{\gamma}_{\max}$) are the clearest illustration of fault rupture. Therefore, $\dot{\gamma}_{\max}$ has been selected for further studies in this paper.

In this research, considering combinations of materials for the sand layers, five dip angle values and two vertical displacements were applied to represent faulting; thus, totally, 60 analyses were carried out as categorized and summarized in Table 3. As a typical legend, Figure 6 introduces refraction angles of rupture in a two-layered soil. Angles, α_1, α_2, and surface angle, α_3, can be measured for different cases of analysis for further investigation.

Typical results are shown in Figure 7, in terms of the contours of maximum shear strain rate for a 60°

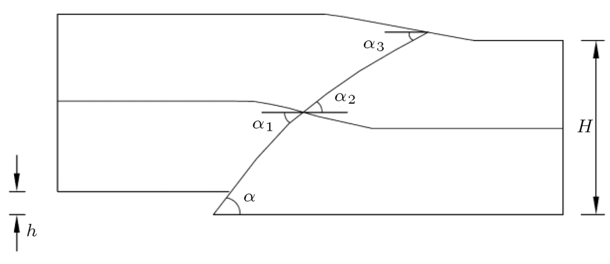

Figure 6. Two-layered soil and refraction angles of rupture.

Table 3. Characteristics of different analyses performed on two-layered sand deposit by numerical modeling.

Analysis No.	α	h/H	Mesh	Layered soil type
1	30	4%	121×40	DS-MS, DS-LS, MS-DS, MS-LS, LS-DS, LS-MS
2	45	4%	121×40	DS-MS, DS-LS, MS-DS, MS-LS, LS-DS, LS-MS
3	60	4%	121×40	DS-MS, DS-LS, MS-DS, MS-LS, LS-DS, LS-MS
4	75	4%	152×40	DS-MS, DS-LS, MS-DS, MS-LS, LS-DS, LS-MS
5	90	4%	152×40	DS-MS, DS-LS, MS-DS, MS-LS, LS-DS, LS-MS
6	30	2%	121×40	DS-MS, DS-LS, MS-DS, MS-LS, LS-DS, LS-MS
7	45	2%	121×40	DS-MS, DS-LS, MS-DS, MS-LS, LS-DS, LS-MS
8	60	2%	121×40	DS-MS, DS-LS, MS-DS, MS-LS, LS-DS, LS-MS
9	75	2%	152×40	DS-MS, DS-LS, MS-DS, MS-LS, LS-DS, LS-MS
10	90	2%	152×40	DS-MS, DS-LS, MS-DS, MS-LS, LS-DS, LS-MS

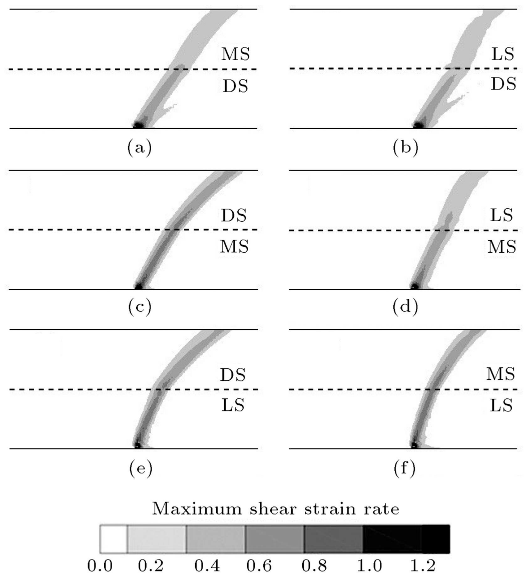

Figure 7. Fault rupture for 60° fault in (a) DS-MS soil, (b) DS-LS soil, (c) MS-DS soil, (d) MS-LS soil, (e) LS-DS soil, and (f) LS-MS soil.

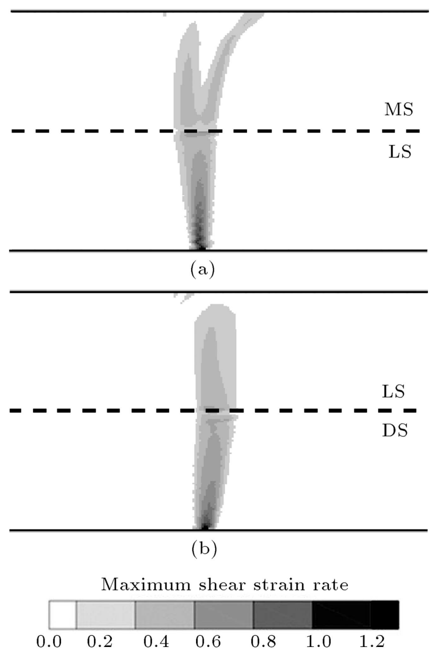

Figure 8. Fault rupture propagation in the form of contours of maximum shear strain rate at 4% base displacement in (a) LS-MS, and (b) DS-LS for 90° fault angle.

fault in (a) DS-MS, (b) DS-LS, (c) MS-DS, (d) MS-LS, (e) LS-DS, and (f) LS-MS soils. For the special case of 90° fault, more results are added in Figure 8 for (a) LS-MS, and (b) DS-LS soils.

4.2. Near surface slope of rupture path

The near surface slope of a rupture path within a uniform horizontal soil layer has received much attention in recent research. Experimental investigations [3] and numerical simulations [24] of reverse faults in sandy soil layers have shown that near the surface, sufficiently far from the imposed boundary conditions of fault displacement, the rupture path follows the failure directions corresponding to that of the passive state in soil. Thus, the rupture path approaches the surface with an angle of $45° - \varphi/2$, with respect to the direction of the maximum principal stress [3], or even more realistically, $45° - \psi/2$ [3,25,26], and therefore, it is almost independent of the fault dip angle.

In this study, an attempt is made to apply theoretical discussions as well as measurement procedures concerning one-layered sands to the upper layer of two-layered ones. Within the two-layered sand, the near surface slopes, α_3 values, are measured and compared with the theoretical values, $\lambda = 45° - \psi_2/2$, as presented in Table 4, while there is an agreement between the values of the two sets.

4.3. Rupture refraction

The orientation of fault rupture alters when passing through the interface of two materials, as depicted

Table 4. The theoretical and measured values for the near surface slope of rupture path and the critical fault dip angle.

Soil arrangement	$\lambda = 45° - \psi_2/2^*$	α_3 (°)	α_{crit} (°)
DS-MS	43.5	47.4	31.5
DS-LS	45	48.2	28.4
MS-DS	42	45.1	34.1
MS-LS	45	49.3	29.1
LS-DS	42	42.5	36.3
LS-MS	43.5	48.1	32.9

* The residual value of ψ_2 has been utilized.

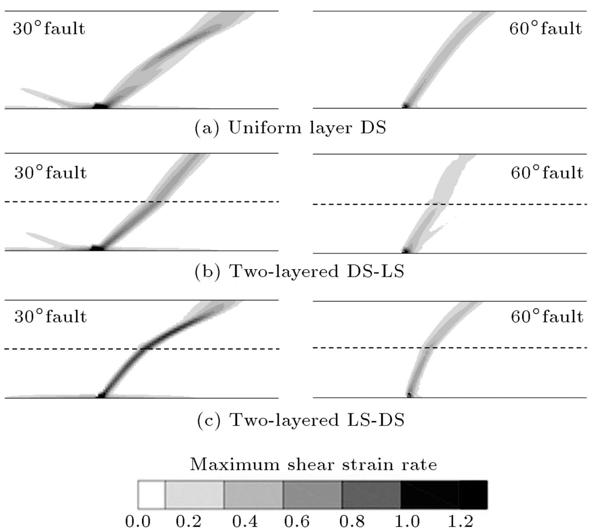

Figure 9. Fault rupture propagation in the form of contours of maximum shear strain rate at 4% base displacement in (a) uniform dense sand DS, (b) two-layered sand DS-LS, and (c) two-layered sand LS-DS for 30° and 60° fault angles.

in Figure 7. This becomes more evident when these results are compared with the corresponding results for one layer sand, as shown in Figure 9.

The shear strength parameters (φ and c) may be employed to find a relationship between soil characteristics and fault refraction at the interface of two sand layers. If the indices 1 and 2 refer to the lower and upper layers, respectively, and if the ratio of shear strengths, τ_2/τ_1, just above and below the interface, is expressed in terms of φ and c and normal stress, σ_n, we have:

$$\frac{\tau_2}{\tau_1} = \frac{(\sigma_n)_2 . \tan\varphi_2 + c_2}{(\sigma_n)_1 . \tan\varphi_1 + c_1}. \tag{6}$$

With $c \approx 0$ for sands and variations of σ_n being negligible in the vicinity of interface [i.e., $(\sigma_n)_1 = (\sigma_n)_2$], Eq. (6) may be summarized as:

$$\frac{\tau_2}{\tau_1} = \frac{\tan\varphi_2}{\tan\varphi_1}. \tag{7}$$

The variations of α_1 and α_2, represented by the quantity of $\tan\alpha_2/\tan\alpha_1$, may be studied against variations of shear strengths immediately above and below the interface, as indicated by Eq. (7). Figure 10 presents the results of different soil arrangements for four fault dip angles. These results suggest:

1. $\tan\alpha_2/\tan\alpha_1$ values for each fault dip versus $\tan\varphi_2/\tan\varphi_1$ values are reasonably fitted to a line, with R^2, square of the correlation coefficient, higher than 90%.
2. For each fault dip angle, $\tan\alpha_2/\tan\alpha_1$ decreases with the increase of $\tan\varphi_2/\tan\varphi_1$, taking values greater than one for the soil arrangements, where the upper layer is looser than the lower layer with values less than one for the soil arrangements where the upper layer is denser than the lower layer. In other words, at the interface of the two sandy materials, the rupture path takes a comparatively steeper orientation within the looser material.
3. The aforementioned best fit line steepens as the fault dip angle increases, i.e. as far as the slope of the rupture path before and after the interface is concerned, refraction is more pronounced for greater fault dip angles.
4. The best fit lines in Figure 10 pass through the point (1, 1), with a minimal error. This indicates that, as expected, when the shear strength parameters of the two layers are similar (i.e. $\tan\varphi_2/\tan\varphi_1 = 1$), the rupture path does not experience any refraction (i.e. $\tan\alpha_2/\tan\alpha_1$ equals 1). Furthermore, $\tan\alpha_2/\tan\alpha_1$ is the most in DS-LS and the least in LS-DS arrangements. This means that refraction is more pronounced when the contrast between the shear strengths of the two soils is higher.

Moreover, as depicted in Figure 8, in the case of 90° fault, α_1 and α_2 are almost 90° and their tangent tends to infinity; therefore, it is almost impossible to locate its results in Figure 10.

4.4. Convexity/concavity of rupture path within the upper layer

As α_2 increases with the increase of α, a critical value of the fault dip angle, α_{crit}, exists for each soil arrangement in which $\alpha_2 = \alpha_3$. Figure 11 shows the typical results for LS-DS soil. From the analyses results, the values of α_{crit} for all the arrangements have been determined and summarized in Table 4.

The relation between α and α_{crit} defines the convexity of the rupture path within the upper layer.

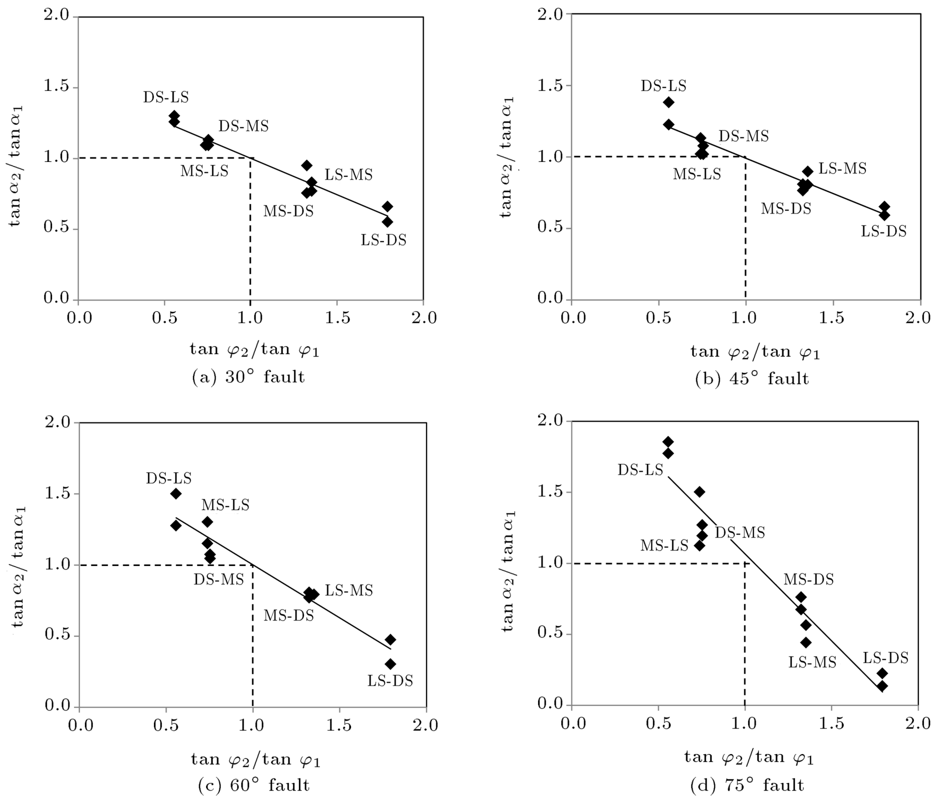

Figure 10. Ratio of tangents of refraction angles versus ratio of tangents of friction angles for (a) 30° fault, (b) 45° fault, (c) 60° fault, and (d) 75° fault.

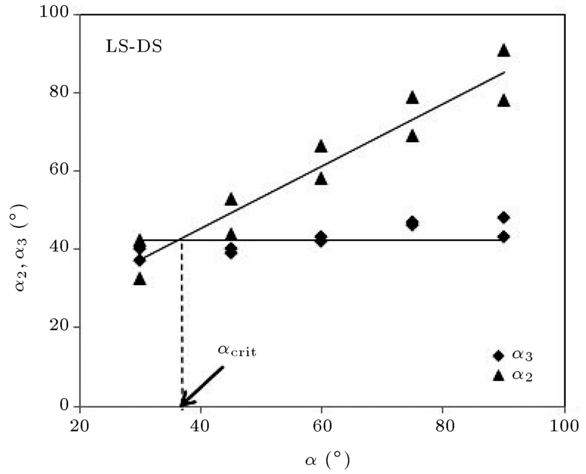

Figure 11. Refraction and surface angles versus fault dip angles for LS-DS soil arrangement.

For $\alpha > \alpha_{crit}$ (which leads to $\alpha_2 > \alpha_3$), this rupture path experiences a convex curve when viewed from the hanging wall. This convex pattern of rupture has been widely perceived in field observations [19], as well as in experimental and numerical simulations [3,5-7]. However, the evidence of the concave rupture path (i.e. $\alpha_2 < \alpha_3$) have been reported in a few experimental and numerical simulations of uniform soil layers [3,9] and also signed in some of the analyses of the present research.

4.5. Discussions on rupture paths in two-layered sands

Based on the ideas presented in Sections 4.3 and 4.4, the patterns of rupture path in two-layered sands may be compiled and presented in a graph, as shown in Figure 12. As far as refraction in the interface of two layers is concerned, two distinct behaviors have been recognized: steepening (Figure 12(a) and (c)) or flattening (Figure 12(b) and (d)) of the rupture path after the interface. In addition, convexity (Figure 12(a) and (b)) or concavity (Figure 12(c) and (d)) of the rupture path in the upper layer is the source of further division. The combinations of these cases provide four different patterns. The above suggested patterns are supported by the direct results from the numerical analysis, as shown in Figure 13. Patterns illustrated in Figure 13(a) to (d) are associated, respectively, with those shown in Figure 12(a) to (d). It should be mentioned that the pattern introduced in Figure 12(c) is observed in very mild fault dip angles.

Based on the above discussions and the results shown in Figures 11 to 13, the above patterns are more scientifically compiled and illustrated in Figure 14. Any desired case of two-layered sand, depending on $\tan\varphi_2/\tan\varphi_1$ and α values, may be located in either of Zones 1 to 4. These zones are associated with the rupture patterns introduced in Figure 12(a) to (d),

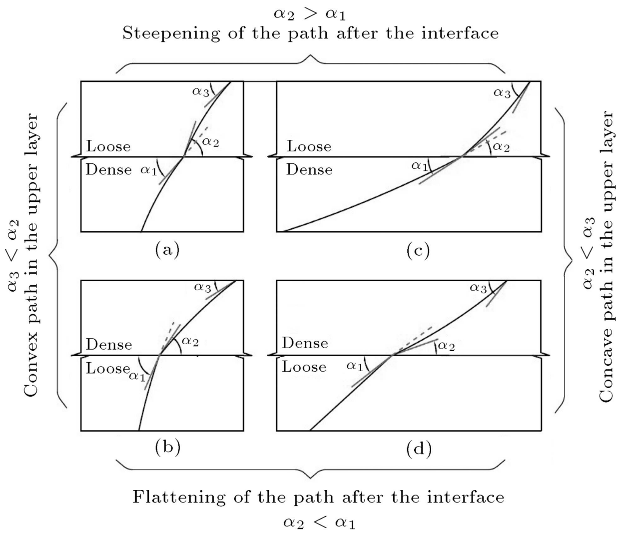

Figure 12. Patterns of fault rupture propagation in two-layered sands: (a) Convex path in the upper layer and steeper path after the interface; (b) convex path in the upper layer and flatter path after the interface; (c) concave path in the upper layer and steeper path after the interface; and (d) concave path in the upper layer and flatter path after the interface.

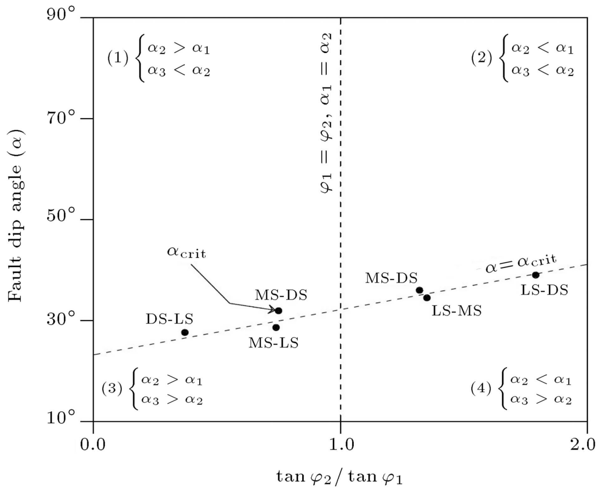

Figure 14. Four zones associated with four rupture patterns in two-layered sand: (1) convex path in the upper layer and steeper path after the interface; (2) convex path in the upper layer and flatter path after the interface; (3) concave path in the upper layer and steeper path after the interface; and (4) concave path in the upper layer and flatter path after the interface.

respectively. Figure 14 indicates that the area under the line $\alpha = \alpha_{\text{crit}}$ is comparatively small, explaining why the concave pattern has been so rarely observed in both field and experimental investigations.

5. Conclusion

In this paper, reverse fault rupture propagation through two-layered sands was studied thoroughly by means of the finite element method. Five fault dip angles (30, 45, 60, 75 and 90 degrees) and three typical sandy soils, which we chose to call dense sand, medium dense sand, and loose sand, were used for this purpose. Combinations of the above sands resulted in six cases for the two-layered sand. The results of the analyses led to the following summarized conclusions:

- General trends of fault rupture propagation, previously reported in physical and numerical simulations of one-layered sand, were found in two-layered sands.
- The surface angle of rupture is almost independent of the fault dip angle and mostly related to the type of upper sand layer.
- The fault rupture path refracts in the interface of the two sand layers with unequal mechanical soil parameters. Refraction depends upon the friction

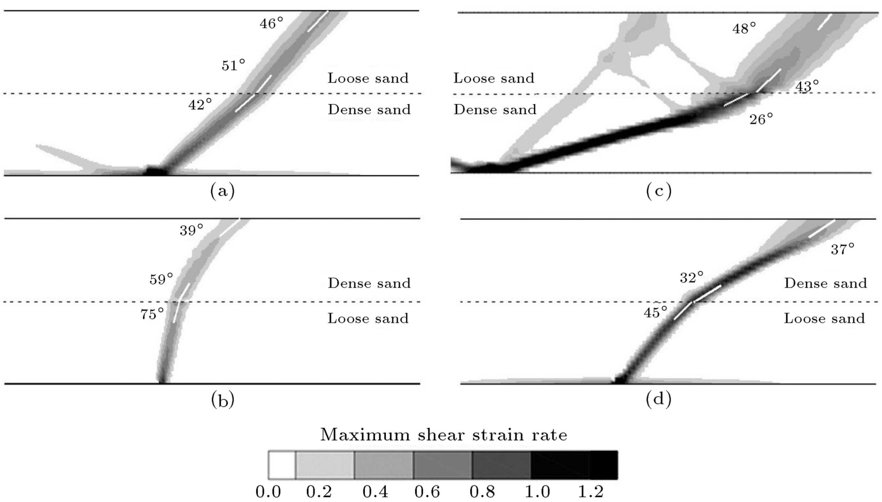

Figure 13. Fault rupture propagation in (a) 30° fault in DS-LS soil, (b) 75° fault in LS-DS soil, (c) 30° fault in LS-DS soil, and (d) 15° fault in DS-LS soil.

angle of soil: The rupture path takes a steeper orientation within the material with lower friction angle, i.e. the looser material.

- Refraction is more noticeable when the two layers differ more with respect to their mechanical parameters. Moreover, refraction is more pronounced for greater fault dip angles.
- The rupture path in the upper layer experiences a convex or concave curve depending upon the relation between fault dip angle and a critical angle (α_{crit}) defined for each soil arrangement.
- When two-layered sands are subjected to reverse fault rupturing initiated from the underlying rock, four different rupture patterns may be observed, depending on the sequence of layering (denser materials over looser materials and vice versa) and the value of the fault dip angle, compared with α_{crit}.

References

1. Bray, J.D., Seed, R.B. and Seed, H.B. "The effect of tectonic movements on stresses and deformations in earth embankments", *Earthquake Engineering Research Center*, University of California at Berkeley, Report No. UCB/EERC-90/13 (1990).
2. Bonilla, M.G. and Lienkaemper, J.J. "Visibility of fault strands in exploratory trenches and timing of rupture events", *Geology*, **18**, pp. 153-156 (1990).
3. Cole, D.A. Jr. and Lade, P.V. "Influence zones in alluvium over dip-slip faults", *Journal of Geotechnical Engineering Division, ASCE*, **110**(5), pp. 599-615 (1984).
4. Lazarte, C.A. "The response of earth structures to surface fault rupture", Ph.D. Thesis, Department of Civil Engineering, Univ. of California, Berkeley (1996).
5. Johansson, J. and Konagai, K. "Fault induced permanent ground deformations-an experimental comparison of wet and dry soil and implications for buried structure", *Soil Dynamics and Earthquake Engineering*, **26**, pp. 45-53 (2006).
6. Lin, M.L., Chung, C.F. and Jeng, F.S. "Deformation of overburden soil induced by thrust fault slip", *Engineering Geology*, **88**, pp. 70-89 (2007).
7. Bray, J.D., Seed, R.B. and Seed, H.B. "Analysis of earthquake fault rupture propagation through cohesive soil", *Journal of Geotechnical Engineering*, **120**(3), pp. 562-580 (1994).
8. Johansson, J. and Konagai, K. "Fault induced permanent ground deformations: Experimental verification of wet and dry soil, numerical findings' relation to field observations of tunnel damage and implications for design", *Soil Dynamics and Earthquake Engineering*, **27**, pp. 938-956 (2007).
9. Anastasopoulos, I., Gazetas, G., Bransby, M.F., Davies M.C.R. and EI Nahas A. "Fault rupture propagation through sand: Finite-element analysis and validation through centrifuge experiments", *Journal of Geotechnical and Geoenvironmental Engineering*, **133**(8), pp. 943-958 (2007).
10. Bransby, M.F., Davies, M.C.R. and El Nahas, A. "Centrifuge modelling of normal fault-foundation interaction", *Bulletin of Earthquake Engineering*, **6**, pp. 585-605 (2008).
11. Bransby, M.F., Davies, M.C.R. and El Nahas, A. "Centrifuge modelling of reverse fault-foundation interaction", *Bulletin of Earthquake Engineering*, **6**, pp. 607-628 (2008).
12. Loukidis, D., Bouckovalas, G.D. and Papadimitriou, A.G. "Analysis of fault rupture propagation through uniform soil cover", *Soil Dynamics and Earthquake Engineering*, **29**, pp. 1389-1404 (2009).
13. Scott, R.F. and Schoustra, J.J. "Nuclear power plant sitting on deep alluvium", *Journal of Geotechnical Engineering, ASCE*, **100**, pp. 449-459 (1974).
14. Roth, W.H., Kalsi, G., Papastamatiou, O. and Cundall, P.A. "Numerical modelling of fault rupture propagation in soils", *Proceedings of the 4th International Conference on Numerical Methods in Geomechanics*, Edmonton, Canada, pp. 487-502 (1982).
15. Walters, J.V. and Thomas, J.N. "Shear zone development in granular materials", *Proceedings of the 4th International Conference on Numerical Methods in Geomechanics*, Edmonton, Canada, pp. 263-274 (1982).
16. Nakai, T., Wood, D.M. and Stone, K.J.L. "Numerical calculations of soil response over a displacing basement", *Soils and Foundations*, **35**(2), pp. 25-35 (1995).
17. Anastasopoulos, I. and Gazetas, G. "Foundation-structure systems over a rupturing normal fault: Part II. Analysis of the Kocaeli case histories", *Bulletin of Earthquake Engineering*, **5**, pp. 277-301 (2007).
18. Yilmaz, M.T. and Paolucci, R. "Earthquake fault rupture shallow foundation interaction in undrained soils: A simplified analytical approach", *Earthquake Engineering and Structural Dynamics*, **36**, pp. 101-118 (2007).
19. Bray, J.D. "Developing mitigation measures for the hazards associated with earthquake surface fault rupture", *Workshop on Seismic Fault-Induced Failures - Possible Remedies for Damage to Urban Facilities*, University of Tokyo Press, pp. 55-79 (2001).
20. Bray, J.D. and Seed, R.B., Cluff L.S. and Seed H.B. "Earthquake fault rupture propagation through soil", *Journal of Geotechnical Engineering*, **120**(3), pp. 543-561 (1994).
21. Lee, J.C., Chen, Y.G., Sieh, K., Mueller, K., Chen, W.S., Chu, H.T., Chan, Y.C., Rubi, C. and Yeats, R. "A vertical exposure of the 1999 surface rupture of the Chekungpu fault at Wufeng, Western Taiwan", *Structural and Paleoseismic Implication for an Active Trust Fault*, Bulletin of the Seismological Society of America, **91**(5), pp. 914-929 (2001).

22. Menetrey, P. and Willam, K. "A triaxial failure criterion for concrete and its generalization", *ACI Structures Journal*, **92**, pp. 311-318 (1995).

23. Abaqus, Inc. (2010). Abaqus V.6.10 user's manual.

24. Mortazavi Zanjani, M., Soroush, A. and Solhmirzaei, R. "Near surface distortion under fault Rupture propagation through soil", *Proceedings of the 1st International Conference on Urban Construction in the Vicinity of Active Faults*, Tabriz, Tehran (2011).

25. Roscoe, K.H. "The influence of strains in soil mechanics", *10th Rankine Lecture, Geotechnique*, **20**(2), pp. 129-170 (1970).

26. James, R.G. and Bransby, P.L. "A velocity field for some passive earth pressure problems", *Geotechnique*, **21**(1), pp. 61- 83 (1971).

Biographies

Mahda Mortazavi Zanjani received a BS degree in Civil Engineering and a MS degree in Earthquake Engineering from the University of Tehran, Iran, in 1999 and 2002, respectively. Currently, she is working on fault rupture propagation in soil layers and earth dams for her PhD degree program.

Abbas Soroush received his BS degree in Civil Engineering in 1984, and an MS degree in Soil Mechanics and Foundation Engineering, in 1987, from Amirkabir University of Technology (AUT), Tehran, Iran. He then obtained his PhD degree in Geotechnical Engineering from the University of Alberta, Canada, in 1996. He is currently Associate Professor in the Department of Civil and Environmental Engineering at AUT, where he served as Chair of the department for four years (2000 to 2005), and president of the Iranian Geotechnical Society. Professor Soroush has lectured a variety of courses at undergraduate and graduate levels, and has supervised more than 75 MSc and 5 PhD students. He has also presented several papers and lectures in international and national Journals, conferences and seminars. Dr. Soroush has been a member of the Executive Board of the Iranian National Committee on Large Dams (IRCOLD, ICOLD), since 2006.